Advanced Ceramics Progress: Vol. 11, No. 1, (Winter 2025) 28-35

Materials and Energy Research Center
MERC

Contents lists available at ACERP

Advanced Ceramics Progress

Journal Homepage: www.acerp.ir

Original Research Article

The Effect of Low Temperature Heat Treatment on the Corrosion Resistance of the Electrodeposited $FeCrNiCuAg_{0.5}$ High Entropy Alloy Coating

Mohamad Sadegh Amiri Kerahroodi [a]*, Masoud Rajabi [b], Mohammad Talafi Noghani [b]

[a] *PhD Candidate, Department of Materials Science and Engineering, Faculty of Technology and Engineering, Imam Khomeini International University (IKIU), Qazvin, Iran.*

[b] *Associate Professor, Department of Materials Science and Engineering, Faculty of Technology and Engineering, Imam Khomeini International University (IKIU), Qazvin, Iran.*

* Corresponding Author Email: sadeghamiri@aol.com (M. S. Amiri Kerahroodi) URL: https://www.acerp.ir/article_225813.html

ARTICLE INFO

Article History:
Received 15 January 2025
Received in revised form 15 June 2025
Accepted 25 July 2025

Keywords:
Multi-Principal Element Alloys,
High-Entropy Alloys,
Retained Strain,
Electroplating ,
316 L Stainless Steel,
Corrosion

ABSTRACT

In this research, a coating composed of the FeCrNiCuAg0.5 compound, a multi-principal element alloy, was applied to the surface of an AISI (American Iron and Steel Institute) 316 stainless steel plate using the DC current electroplating technique in an aqueous bath. The coated sample was subjected to heat treatment at 200 °C in ambient atmosphere. The corrosion resistance of the samples was studied through polarization and immersion corrosion tests. Field Emission Scanning Electron Microscopy (FESEM) revealed improved corrosion resistance, and X-Ray Diffraction (XRD) patterns showed slight shifts to the right. The results indicated a 24% reduction in corrosion current. Further investigation suggested that this improvement was due to stress relief after the low-temperature heat treatment. Residual stresses caused by electroplating create local anodic and cathodic sites, and relieving these stresses removes this effect. Achieving corrosion resistance in an electrodeposited HEA coating through a simple and inexpensive heat treatment represents a novel approach, which could be explored in greater detail in future research, such as by investigating a wider range of temperatures.

https://doi.org/10.30501/acp.2025.431929.1173

1. INTRODUCTION

New Multi-Principal Element Alloys (MPEA) have attracted increasing attention in the field of alloy design and manufacturing. These alloys typically consist of 3 to 6 elements in almost the same molar ratios, offering a wide compositional diversity that did not exist before. A special category of MPEA alloys is High Entropy Alloys (HEAs), which contain at least 5 or more constituent elements in almost equal molar ratios. These materials exhibit unique properties (Senkov, Miller et al. 2015). Their microstructure appears to consist of random arrangement of different atoms in a solid solution phase which causes a local disorder, hence remarkable corrosion resistance (Shi, Yang et al. 2017). It seems that these disordered areas prevent the formation of localized anodes and cathodes. Studies on the corrosion behavior of HEAs in different environments reveals that if these alloys contain passivation elements such as chromium, nickel, and molybdenum, they can exhibit corrosion resistance comparable to, or even superior to, base metal alloys (Shi, Yang et al. 2017). A variety of methods have been developed to fabricate a high entropy alloy, including vacuum evaporation, arc melting and casting under vacuum, electron beam evaporation and ion sputtering, laser coating, and powder metallurgy (Yousefi, Rajabi et al. 2023). A less explored method is

Please cite this article as: Amiri Kerahroodi, M. S. , Rajabi, M. & Talafi Noghani, M. (2025). The Effect of Low Temperature Heat Treatment on the Corrosion Resistance of the Electrodeposited $FeCrNiCuAg_{0.5}$ High Entropy Alloy Coating, *Advanced Ceramics Progress*, 11(1), 28-35. https://doi.org/10.30501/acp.2025.431929.1173

electrochemical deposition, as demonstrated by Yao Chen for HEA syntheis (Yao, Zhang et al. 2008). In addition to the low cost and simplicity of the plating process itself (Gurrappa and Binder 2008, Kaveh et al. 2023), employing HEAs as coatings is more economical than uisng them as bulk materials, given their comparatively higher production cost (Shi, Yang et al. 2017). HEA coatings function as protective barriers by forming stable passive films that inhibit corrosion. Their surface layers provide high ionic resistance which supresses electrochemical reactions. This synergistic behavior grants HEAs remarkable resistance to pitting erosion, particularly in saline environments (Shi, Yang et al. 2017).

The current study investigates the use of under-researched alloy to create a coating of a multi-element alloy with the composition of $FeCrNiCuAg_{0.5}$. This coating is expected to provide the excellent corrosion resistance properties typical of HEA alloys, while its surface status makes it more economical than bulk material. At the same time, since the alloy contains both copper and silver, it has the potential to exhibit strong antibacterial effect (Lin, Vidic et al. 1996, Hahn, Günther et al. 2011, Hans, Támara et al. 2014, Khalili, et al. 2020). However, the the antibacterial properties of this coating are not within the scope of this article; instead, the focus is on examining the effect of low-temperature heat treatment on the corrosion resistance of the plated coating through polarization tests, immersion studies, and XRD and FESEM analyses. To the best of the authors' knowledge, this is the first study to report the effect of low-temperature heat treatment on the corrosion resistance of amorphous $FeCrNiCuAg_{0.5}$ high-entropy alloy coatings produced by electrodeposition. This work introduces a simple, low-cost, and scalable surface modification strategy applicable to amorphous electrodeposited HEAs, which may be particularly useful in industries such as marine engineering, biomedical devices, or chemical processing, where enhanced surface durability and corrosion resistance are essential, and the use of bulk HEAs is economically unfeasible.

Similar improvements in corrosion resistance have been reported for pulsed-electrodeposited nickel coatings after low-temperature heat treatment, where stress relaxation and surface homogenization contributed to enhanced electrochemical performance (Khiabani, Seyedraoufi & Heydarzadeh Sohi 2021).

2. MATERIALS AND METHODS

2.1. Electroplating process

For electroplating, a 316 stainless steel substrate was used as cathode, and graphite as the anode. The plate samples were cut in dimensions of 1 cm × 6 cm × 1 mm as cathode specimen. The samples were then polished with sand papers ranging from 200- to 3000-grit. The graphite anode had an area 2.5 times larger than that of cathode, and the interelectrod distance was maintained as 3 cm. The degreasing process was carried out in a mixed solution containing NaOH 20g/L, $NaCO_3$ 30g/L and $NaPO_4$ 40g/L at a temperature of 60°C. The samples were then immersed in pure water for five minutes, followed by a five-minute immersion in 5% HCl solution. Next, they were immersed again in pure water and dried. Since the passive layer of Cr_2O_3 on the surface of stainless steel acts as a barrier to the adhesion of electroplated coating, the surface of the stainless steel must be free of passive layer using a strike solution (Kumarasiri, Amarasinghe et al. 2020) for 30 seconds; immediately afterwards, the current was reversed, and a nickel layer was applied for three minutes. The strike solution contains 240000 (g/m^3) of $NiCl_2(6H_2O)$ and 80000 (g/m^3) of HCl. According to the authors' observations, the removal of the passive layer (during the anodic reaction) should be done in a mixed mode prevent pitting, while the deposition of the nickel layer (during the cathode reaction) should be conducted under still conditions so that the nickel layer is applied uniformly. As electroplating can be done in either acidic or basic baths (Walsh and Low 2016), an acidic bath was selected for this study. Table 1 shows the composition of electroplating bath, and the pH was adjusted to approximately 3.5 using HCl. All metal salts used in electroplating bath were dried at the temperature of 185°C for 12 hours to remove any moisture prior to weighing and adding to distilled water. All chemical material were of pure (99.9%) grade. After adding chemical materials to distilled water at the concentrations listed in Table 1, the bath was heated to 60°C, mixed at 400 rpm for 3 hours, and then cooled to room temperature for 24 hours. The electroplating process was carried out at a current density of $28mA/cm^2$ at room temperature.

TABLE 1. Composition of water electroplating bath

Material (salts)	$CrCl_2$	$NiCl_2$	$FeCl_2$	$CuCl_2$	AgCl
Concentration (mol/Lit)	0.3	0.1	0.01	0.015	0.08
Material (additive)	NaBr	NH_4Cl	H_3BO_3	Sodium citrate	Thiourea
Concentration (mol/Lit)	1.5	0.9	0.5	0.5	0.1

2.2. Heat treatment and other evaluation tests

A series of samples were placed in a furnace under ambient atmosphere at a temperature of 200°C for one hour and then cooled inside the furnace. Polarization measurements were performed in a 3.5% NaCl solution at room temperature using a CHI 604E instrument. A saturated calomel and a platinum foil served as the reference electrode and counter electrode, respectively. A stainless steel (SS 316 L) substrate, with an exposed area of 1 cm^2, was used as the working electrode for corrosion tests conducted in the same 3.5% NaCl solution. The potentiodynamic polarization test (Princeton Applied Research, USA) was repeated three times. The potential range for this experiment was from -800mV to 1000mV.

X-ray diffraction analysis was carried out for the uncoated, coated and heat-treated samples through conventional XRD (JEOL, JDX-3530 M, Czech) and grazing (Bourevestnik, DRON-8, Russia) techniques. The conventional XRD experiments were conducted using assessment of Cu-Kα radiation, with a voltage and current and of 40 kV and 40 mA, respectively. Data for diffraction patterns were collected over a 2θ range of 30°-80°, with a step size of 0.02◦. Grazing XRD experiments were performed under the same radiation, voltage, and current conditions, with data collected in a 2θ range of 20°-80°, a step size of 0.02◦, and a grazing incidence angle of 1°.

The heat-treated and non-heat-treated samples were subjected to corrosion immersion test in a 3.5% NaCl solution for one month. The surface morphology of all four sample conditions, i.e., heat-treated, non-heat-treated, immersed, and non-immersed, were examined using FESEM electron microscope (Make: TESCAN, Czech; Model: Mira 3-XMU).

3. RESULTS AND DISCUSSION

3.1. Xrd results

Conventional XRD patterns for the uncoated and coated sheets, both before and after heat-treatment, are shown in Figure 1. Obviously, the peak patterns correspond to those of the substrate, representing FCC phases (Leicht, Pauzon et al. 2021) of AISI 316 stainless steel. The patterns observed in the (111), (020), and (022) plates at 43.4, 50.6, and 74.3 2Ɵ degree angles (with the 96-901-5072 number as a reference code) confirms the presence of FCC phase, which is attributed to 316 austenitic stainless steel (Leicht, Pauzon et al. 2021). Most published studies (Yao, Zhang et al. 2008, Chenzhong, Bohui et al. 2011, Li, Sun et al. 2014, Soare, Burada et al. 2015, Zhu, Meng et al. 2022) report that high-entropic alloy coatings exhibit a primarily amorphous structure. However, contrasting results were found by Yoosefan et al., who reported a cubic FCC single solid solution for the surface structure of their electrodeposited coating (Dehestani, Sharafi et al. 2022). Furthermore, Dehestani et al.'s research indicated that although the dominant phase was amorphous, trace amounts of nano crystalline FCC phases were also present on the coating (Yoosefan, Ashrafi et al. 2020). Based on the findings of some researchers, the absence of coating-specific peaks indicates the amorphous nature of the coatings (Yao, Zhang et al. 2008, Li, Sun et al. 2014, Soare, Burada et al. 2015). Figure 2 presents the SEM cross-sectional image of coated specimen, suggesting that the coating thickness is less than detection limit of the conventional XRD. The grazing XRD was used to provide more information. Figure 3 shows the results for both both heat-treated and non-heat-treated coatings. As observed, all coatings exhibit an amorphous structure. This indicates that heat treatment at a temperature of 200°C has no effect on the crystallization of the coating or the formation of intermetallic phases or solid solution phases. In addition, no significant oxidation or crystallization was observed as a result of the heat treatment.

3.2. Corrosion experiment result

In the field of materials testing, the most commonly used method to assess corrosion resistance is the potentiodynamic polarization test. This test determines two vital values, i.e., the corrosion potential (E_{corr}) and the corrosion current (I_{corr}), from the experimental results (Shi, Yang et al. 2017). In this research, the corrosive agent is the chloride anion which can adhere to the meta surface and induce corrosion. The only defense against this is the formation of a passive layer in the form of an oxide, which must be capable of withstanding chloride anion penetration. The effectiveness of this passive layer depends on the presence of alloy elements that enhance its protective capacity (Shi, Yang et al. 2017).

Figure 4 shows the polarization diagram for heat-treated and non-heat-treated coating samples. As seen in Figure 4, the corrosion behavior of the substrate (SS 316) is completely different from that of both heat-treated and non-heat-treated coatings. Corrosion resistance increases after heat treatment. The main parameters shown in Figure 4 were calculated and are presented in Table 2. The results indicate a 24% reduction in the corrosion current and a 45% increase in the polarization resistance.

To compare the corrosion parameters of the current coating with those reorted by other researchers on the corrosion resistance of high entropy alloys, Table 3 is presented. The corrosion resistance of the coating falls within the range of MPEA alloys tested in NaCl solution at room temperature. It should be noted that the alloy coating produced in this research was amorphous (see Figure 3), while the alloys listed in Table 3 were either as-cast or electrodeposited. In addition to the chemical compound, factors such as crystallinity and phase segregation (Senkov, Miller et al. 2015, Qiu, Thomas et al. 2017, Zhang, Yan et al. 2020) can reduce corrosion resistance in as-cast specimens. Surface defects can have the same effect for the electrodeposited references (Popescu, Branzoi et al. 2021). Since the current heat treatment did not cause crystallization, the observed improvement in corrosion resistance cannot be attributed to crystallinity. The polarization curves of both coating seems to show pseudo passive behavior (Lu 2023).

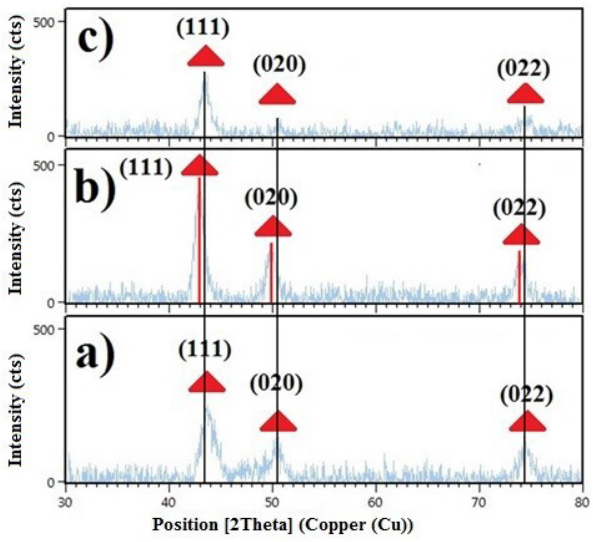

Figure 1. Conventional XRD patterns of a) without coating specimen, b) coated specimen and c) coated specimen after heat treatment.

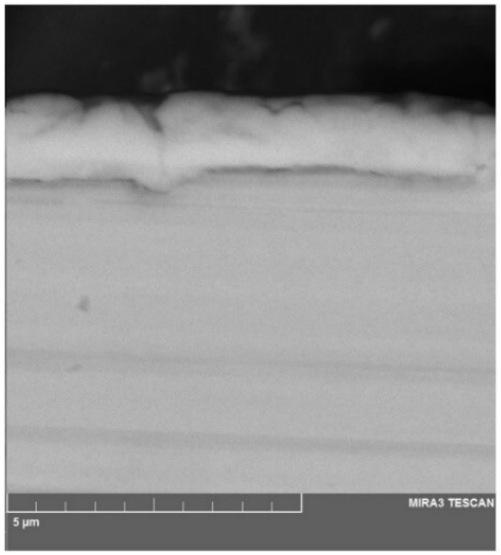

Figure 2. SEM image from cross section of coated specimen.

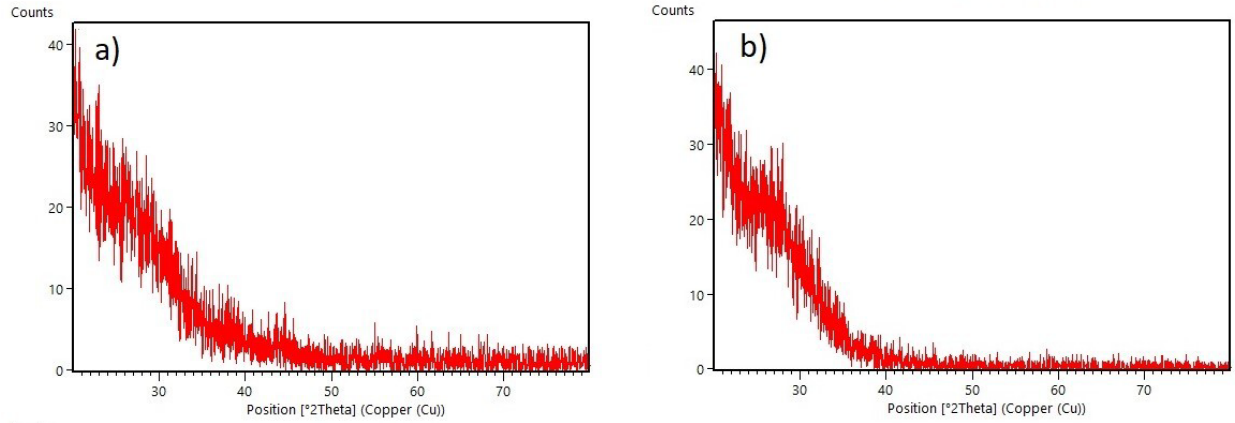

Figure 3. Conventional XRD patterns of a) without coating specimen, b) coated specimen, and c) coated specimen after heat treatment.

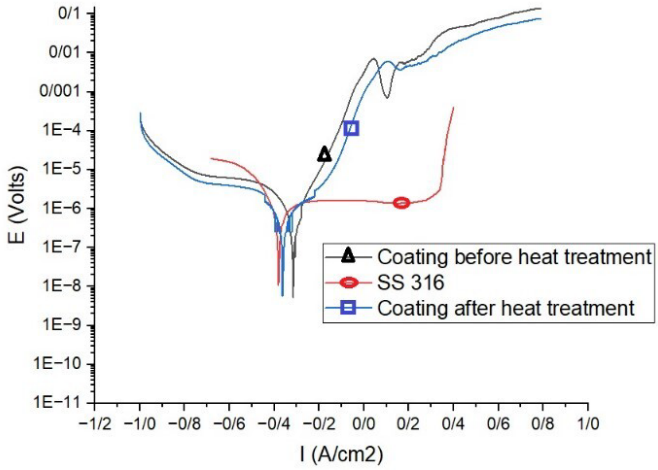

Figure 4. Potentio dynamic polarization diagram for substrate (SS 316) and coated specimens before and after heat treatment.

TABLE 2. Main parameters of corrosion extracted from Figure 4.

Material	I_{corr} A/cm^2	E_{corr} Volts	β_c mV/dec	β_a mV/dec	R_p Ohm*cm^2
SS 316	10.2E-7	-0.381	143.22	242.17	54579
Coating before heat treatment	8.5E-7	-0.315	204.08	169.7	31358
Coating after heat treatment	6.5E-7	-.3636	154.16	239.32	56864

TABLE 3. Polarization test characteristics of some MPEA alloys in different NaCl solution at room temperature based on hydrogen standard reference electrode.

Alloy (Reference)	Solution	E_{corr} (V_{SHE})	i_{corr} (μA/cm^2)	Method
AlFeCoNiCu (Aliyu and Srivastava 2019a)	0.6 M NaCl	-0.78	102	Electroplating
MnCrFeCoNi (Aliyu and Srivastava 2019b)	0.6 M NaCl	-0.84	43.44	Electroplating
CuFeNiCoCr (Aliyu, Rekha et al. 2019d)	0.6 M NaCl	-0.881	101	Electroplating
AlCrFeCoNiCu (Aliyu and Srivastava 2019c)	0.6 M NaCl	-0.717	93.67	Electroplating
FeCoNiCrCu (Hsu, Chiang et al. 2005)	0.6 M NaCl	-0.53	1.23	Arc Melting
$Co_{1.5}CrFeNi_{1.5}Ti_{0.5}$ (Chou, Yeh et al. 2010)	1 M NaCl	-0.44	0.57	Melting
$FeCrNiCuAg_{0.5}$ (Coating-after heat treatment)	0.6 M NaCl	-0.61	0.65	Electroplating
$FeCrNiCuAg_{0.5}$ (Coating-before heat treatment)	0.6 M NaCl	-0.56	0.86	Electroplating

3.3. FESEM studies

The overall EDS analysis shown in Figure 5 was conducted on the coated surface at 4 different points (Figure 5(a)). One representative EDS spectrum analysis is shown in the Figure 5(b), and the average results are presented in Table 4 in terms of atomic percentage. When these values are substituted into Eq. 1, the calculated configuration entropy value exceeds 1.52R, which indicates that the coating alloy is in the range of high entropy alloys (Miracle and Senkov 2017). Eq. 1 (Miracle and Senkov 2017):

$$\Delta S_{mix}^{conf} = -R \sum_{i=1}^{n} x_i \ln (x_i) \quad (1)$$

where ΔS is configuration entropy, R the universal molar gas constant equal to R = 8.314J·mol^{-1}·K^{-1}, and x_i the molar percent ratio of the i_{th} element. Figure 6 (a-d) displays the surfaces of non-heat-treated and heat-treated coated samples before and after the immersion test, respectively. As seen, before the immersion test, the surface morphology of both non-heat-treated (Figure 6 (a)) and heat-treated samples (Figure 6 (b)) shows not significant difference. After the immersion test, the surface of the heat-treated sample (Figure 6 (d)) is not significantly different from that of the non-immersed sample (Figures 6(a) and 6(b)), showing a uniform corrosion. In contrast, in the non-heat-treated sample (Figure 6 (c)), after the immersion test, areas of spherical and cluster morphologies remain, while the surrounding area appear flatted and depleted due to corrosion. Further analysis is required to clarify the role of alloying elements in the corrosion behavior of these materials. A more comprehensive discussion is provided in the results analysis section.

3.4. Analysis of results

The presence of chromium in MPEA alloys plays a proven role as the primary surface passivation agent by forming a protective oxide layer (Cr_2O_3) on the surface (Qiu, Thomas et al. 2017). Nickel also contributes positively to corrosion resistance, particularly by stabilizing chromium in the austenite phase (Qiu, Thomas et al. 2017). Furthermore, alloying nickel with elements such as chromium and copper can produce saltwater-resistant systems like Monel (Ni-Cu) (Qiu, Thomas et al. 2017). The role of copper is more complex. Since the mixing enthalpy of copper with elements such as iron, nickel, and chromium is positive (Qiu, Thomas et al. 2017), it can cause micro-galvanic corrosion in cast alloys due to segregation. On the other hand, the presence of copper in the composition promotes more cathodic kinetics in the alloy (Qiu, Thomas et al. 2017). However, the hypothesis of phase segregation does not convincingly explain the differences in corrosion resistance observed in the present study. This is because the heat treatment temperature used in this research is not within the dissolution range and was insufficient to cause phase separation, an outcome that would have worsened the corrosion behavior. The primary effect of the applied heat treatment is a reduction in residual stresses on the coating surface at low temperatures. A uniform microstructure with reduced galvanic coupling can enhance the corrosion resistance of coatings (Aliyu and Srivastava 2019b, Aliyu and Srivastava 2019c). Nevertheless, defects and imperfections in the structure of electrodeposited films may compromise their performance when exposed to aggressive electrolyte solutions over extended periods (Popescu, Branzoi et al. 2021). Additionally, studies show that the microstructural and chemical homogeneity of coatings is influenced by several factors affecting the overall composition (Yoosefan, Ashrafi et al. 2022). Based on these findings, previous research suggests that uniformity, along with the presence of surface defects, is a critical parameter controlling corrosion resistance. Electroplating at high currents can introduce residual stresses that interfere with microstructural uniformity.

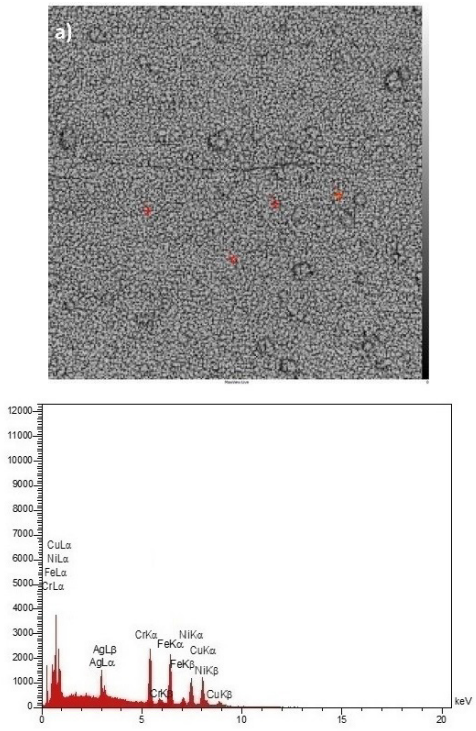

Figure 5. EDS analysis from the surface of coated sample: a) 4 points selected for EDS, and b) EDS diagram of one of the mentioned points.

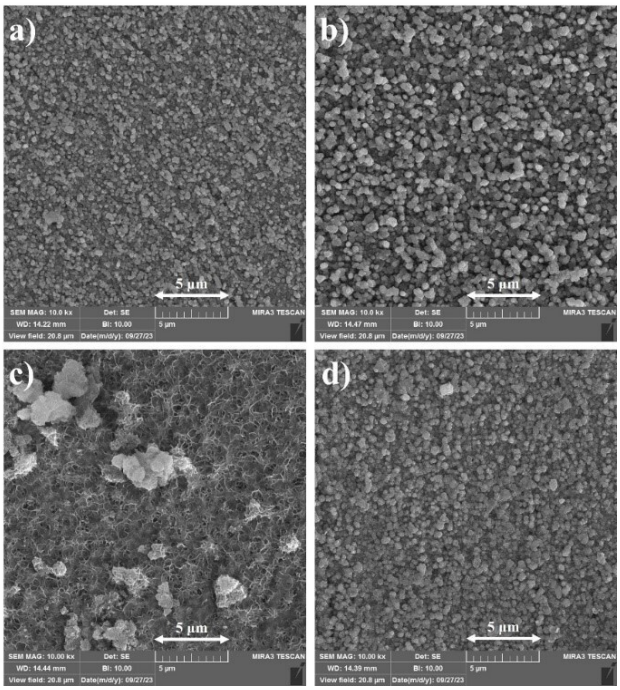

Figure 6. FESEM surface image of coated specimens: a) not heat-treated specimen before immersion test, b) heat-treated specimen before immersion test, c) not heat-treated specimen after immersion test and d) heat-treated specimen after immersion test.

TABLE 4. Overall EDS analysis of the coating surface in terms of atomic percentage

Element	Cr	Fe	Ni	Cu	Ag
Atomic percent	22.29	22.53	21.58	21.55	12.05

The presence of residual stress in plated nickel layers has been widely investigated using various techniques (Kilinc, Unal et al. 2015). In the current research, nickel is included in the coating composition, and a nickel substrate is created during surface activation via the strike solution. Pina et al. studied the residual stresses induced by chromium plating and reported tensile stresses (Pina, Dias et al. 1997). These stresses originate from hydrogen gas evolution during the chrome plating process. Sheikh used XRD to investigate residual stress and concluded that it is a suitable method for this purpose (Sheikh and Noyan 1989). Lin et al. observed that tensile residual stress on plated surfaces negatively affects corrosion resistance (Lin, Liu et al. 2020). Wang et al. demonstrated that low-temperature heat treatment can release residual stress and thereby improve corrosion resistance (Wang, Zhang et al. 2020). X-ray Diffraction (XRD) is a versatile technique for analyzing residual stress in materials, particularly those with crystalline structures (Anderoglu 2005). It measures the distance between crystallographic planes (d-spacing) as an indicator of strain (Anderoglu 2005). This method is applicable to crystalline, polycrystalline, and semi-crystalline materials (Anderoglu 2005). Under tensile stress, the d-spacing increases; under compressive stress, it decreases (Anderoglu 2005). The corresponding shift in the XRD peak position enables the measurement of residual stress (Anderoglu 2005). According to Bragg's law, an increase in the d-spacing results in a leftward shift in the XRD peak position, whereas a decrease causes the peak to shift to the right. lthough the coating is amorphous (see Figure ٢), some residual stress effects appear to have transferred to the substrate surface due to the coating's adherence. Therefore, while the precise value of residual stress cannot be determined solely from the XRD peak shift, its presence can be confirmed. In Figure 1, the difference between the black and red lines indicates a variation in stress status between heat-treated coatings and base samples compared to the coated specimen. The red lines indicate tensile residual stress in the coated sample, as evidenced by the leftward peak shifts. Bragg's equation (Anderoglu 2005), see Eq. 2:

$$2d_{hkl} \times \sin\theta_{hkl} = \lambda \quad (2)$$

Consequently, the reduction of residual tensile strains resulting from electroplating through low-temperature heat treatment accounts for the observed improvement in corrosion resistance. This low-temperature treatment appears to act as a surface modification method that enhances the corrosion properties of materials (Mozetič 2019), which needs further investigations in future studies, particularly in the case of electrodeposited high entropy alloy. The presence of copper in the $FeCrNiCuAg_{0.5}$ coating plays a complex role in corrosion behavior. While copper can promote micro-galvanic corrosion in cast or crystalline alloys due to its positive mixing enthalpy with iron, nickel, and chromium, this effect is significantly diminished in the amorphous state. In the current study, the electrodeposited coating remained amorphous both before and after heat treatment, as confirmed by grazing incidence XRD analysis. This amorphous structure facilitates a more uniform distribution of constituent elements, including copper, thereby minimizing the formation of localized anodic and cathodic sites that drive micro-galvanic activity. Furthermore, the applied low-temperature heat treatment at 200 °C did not induce crystallization or phase segregation but rather alleviated residual tensile stresses introduced during electroplating. The observed shift in the XRD peak position and the improvement in electrochemical parameters such as I_{corr}, and polarization resistance collectively support this conclusion. Therefore, the enhancement in corrosion resistance can be attributed to stress relaxation within the amorphous matrix, without compromising structural homogeneity (Wang et al., 2020; Yoosefan et al., 2020).

4. CONCLUSIONS

Electrodeposition of $FeCrNiCuAg_{0.5}$ alloy on 316L stainless steel resulted in the formation of an amorphous surface layer, as confirmed by grazing XRD analysis.

Low-temperature heat treatment at 200 °C significantly improved the corrosion resistance of the amorphous HEA coating in 3.5% NaCl solution, as evidenced by:

- A 24% reduction in corrosion current density (I_corr),
- A 45% increase in polarization resistance (R_p) compared to the untreated coating.

FESEM images confirmed that a uniform corrosion morphology was preserved after long-term immersion in saline solution, particularly in heat-treated samples, indicating improved structural stability.

The enhancement in corrosion resistance is attributed to the relief of residual tensile stresses induced during electroplating. The XRD peak shift after annealing indicates partial stress relaxation without signs of crystallization or phase segregation. These findings suggest that a simple and cost-effective low-temperature annealing process can enhance the durability of amorphous HEA coatings without compromising structural homogeneity, making them suitable for industrial applications in aggressive environments.

ACKNOWLEDGEMENTS

The authors thank Dr. Nayereh Askari for her support in providing a suitable platform for conducting the experiments in this research.

REFERENCES

1. Aliyu, A., & Srivastava, C. (2019a). Microstructure and corrosion performance of AlFeCoNiCu high entropy alloy coatings by addition of graphene oxide. *Materialia*, *8*, 100459. https://doi.org/10.1016/j.mtla.2019.100459
2. Aliyu, A., & Srivastava, C. (2019b). Microstructure and corrosion properties of MnCrFeCoNi high entropy alloy-graphene oxide composite coatings. *Materialia*, *5*, 100249. https://doi.org/10.1016/j.mtla.2019.100249
3. Aliyu, A., & Srivastava, C. (2019c). Microstructure-corrosion property correlation in electrodeposited AlCrFeCoNiCu high entropy alloys-graphene oxide composite coatings. *Thin Solid Films*, *686*, 137434. https://doi.org/10.1016/j.tsf.2019.137434
4. Aliyu, A., Rekha, M. Y., & Srivastava, C. (2019d). Microstructure-electrochemical property correlation in electrodeposited CuFeNiCoCr high-entropy alloy-graphene oxide composite coatings. *Philosophical Magazine*, *99*(6), 718-735. https://doi.org/10.1080/14786435.2018.1554915
5. Anderoglu, O. (2005). *Residual stress measurement using X-ray diffraction* (Doctoral dissertation, Texas A&M University). https://hdl.handle.net/1969.1/1507
6. Chenzhong, Y., Bohui, W., Zhang, P., Xihong, L., Peng, L., & Yexiang, T. (2011). Facile preparation and magnetic study of amorphous Tm-Fe-Co-Ni-Mn multicomponent alloy nanofilm. *Journal of rare earths*, *29*(2), 133-137. https://doi.org/10.1016/S1002-0721(10)60418-8
7. Chou, Y. L., Yeh, J. W., & Shih, H. C. (2010). The effect of molybdenum on the corrosion behaviour of the high-entropy alloys Co1. 5CrFeNi1. 5Ti0. 5Mox in aqueous environments. *Corrosion Science*, *52*(8), 2571-2581. https://doi.org/10.1016/j.corsci.2010.04.004
8. Dehestani, M., Sharafi, S., & Khayati, G. R. (2022). The effect of pulse current density on the microstructure, magnetic, mechanical, and corrosion properties of high-entropy alloy coating Fe–Co–Ni–Mo–W, achieved through electro co-deposition. *Intermetallics*, *147*, 107610. https://doi.org/10.1016/j.intermet.2022.107610
9. Gurrappa, I., & Binder, L. (2008). Electrodeposition of nanostructured coatings and their characterization—a review. *Science and Technology of Advanced Materials*. https://doi.org/10.1088/1468-6996/9/4/043001
10. Hahn, A., Günther, S., Wagener, P., & Barcikowski, S. (2011). Electrochemistry-controlled metal ion release from silicone elastomer nanocomposites through combination of different metal nanoparticles. *Journal of Materials Chemistry*, *21*(28), 10287-10289. https://doi.org/10.1039/C0JM04480F
11. Hans, M., Támara, J. C., Mathews, S., Bax, B., Hegetschweiler, A., Kautenburger, R., Solioz, M., Mücklich, F., (2014). Laser cladding of stainless steel with a copper–silver alloy to generate surfaces of high antimicrobial activity. *Applied Surface Science*, *320*, 195-199. https://doi.org/10.1016/j.apsusc.2014.09.069
12. Hsu, Y. J., Chiang, W. C., & Wu, J. K. (2005). Corrosion behavior of FeCoNiCrCux high-entropy alloys in 3.5% sodium chloride solution. *Materials Chemistry and Physics*, *92*(1), 112-117. https://doi.org/10.1016/j.matchemphys.2005.01.001

13. Kaveh, M., Sajjadnejad, M., Mohassel, A., & Setoudeh, N. (2023). Influence of B4C Nanoparticles on Corrosion Characteristics of Ni Matrix Nanocomposite Coatings Fabricated via Pulse Electroplating Technique. Advanced Ceramics Progress, 9(3), 16-30. https://doi.org/10.30501/acp.2024.429141.1141

14. Khalili, A., Naeimi, F., & Fakhrizadeh, A. A. (2020). Electrodeposited hydroxyapatite/graphene oxide/zirconia oxide composite coatings: Characterization and antibacterial activity. Advanced Ceramics Progress, 6(4), 8-14. https://doi.org/10.30501/acp.2020.233349.1037

15. Khiabani, A., Seyedraoufi, Z. S., & Heydarzadeh Sohi, M. (2021). Heat Treatment of Pulsed Electroplated Nickel Deposited on AA2024 Aluminum. Advanced Ceramics Progress, 7(1), 46-51. https://doi.org/10.30501/acp.2021.252211.1048

16. Kilinc, Y., Unal, U., & Alaca, B. E. (2015). Residual stress gradients in electroplated nickel thin films. *Microelectronic Engineering*, *134*, 60-67. https://doi.org/10.1016/j.mee.2015.01.042

17. Kumarasiri, A., Amarasinghe, D. A. S., & Attygalle, D. (2020). Surface wettability Analysis of nichrome alloy based on the measurements of sessile droplet contact angles. In *2020 Moratuwa Engineering Research Conference (MERCon)* (pp. 160-164). IEEE. https://doi.org/10.1109/MERCon50084.2020.9185360

18. Leicht, A., Pauzon, C., Rashidi, M., Klement, U., Nyborg, L., & Hryha, E. (2021). Effect of part thickness on the microstructure and tensile properties of 316L parts produced by laser powder bed fusion. *Advances in Industrial and Manufacturing Engineering*, *2*, 100037. https://doi.org/10.1016/j.aime.2021.100037

19. Li, H., Sun, H., Wang, C., Wei, B., Yao, C., Tong, Y., & Ma, H. (2014). Controllable electrochemical synthesis and magnetic behaviors of Mg–Mn–Fe–Co–Ni–Gd alloy films. *Journal of Alloys and Compounds*, *598*, 161-165. https://doi.org/10.1016/j.jallcom.2014.02.051

20. Lin, L., Liu, Z., Zhuang, W., & Peng, H. (2020). Effects of pre-strain on the surface residual stress and corrosion behavior of an Al-Zn-Mg-Cu alloy plate. *Materials Characterization*, *160*, 110129. https://doi.org/10.1016/j.matchar.2020.110129

21. Lin, Y. S. E., Vidic, R. D., Stout, J. E., & Victor, L. Y. (1996). Individual and combined effects of copper and silver ions on inactivation of Legionella pneumophila. *Water Research*, *30*(8), 1905-1913. https://doi.org/10.1016/0043-1354(96)00077-2

22. Lu, X. (2023). Determination Methods of Passivation. In Passivation and Corrosion of Black Rebar with Mill Scale (pp. 17-25). Singapore: Springer Nature Singapore. https://doi.org/10.1007/978-981-19-8102-9_2

23. Miracle, D. B., & Senkov, O. N. (2017). A critical review of high entropy alloys and related concepts. *Acta materialia*, *122*, 448-511. https://doi.org/10.1016/j.actamat.2016.08.081

24. Mozetič, M. (2019). Surface modification to improve properties of materials. Materials, 12(3), 441. https://doi.org/10.3390/ma12030441

25. Pina, J., Dias, A., Francois, M., & Lebrun, J. L. (1997). Residual stresses and crystallographic texture in hard-chromium electroplated coatings. *Surface and coatings technology*, *96*(2-3), 148-162. https:/doi.org/10.1016/S0257-8972(97)00075-3

26. Popescu, A. M. J., Branzoi, F., , Constantin, I., Anastasescu, M., , Burada, M., Mitrică, D., Anasiei, I., Olaru, M. T., and Constantin, V., (2021). Electrodeposition, characterization, and corrosion behavior of CoCrFeMnNi high-entropy alloy thin films. *Coatings*, *11*(11), 1367. https://doi.org/10.3390/coatings11111367

27. Qiu, Y., Thomas, S., Gibson, M. A., Fraser, H. L., & Birbilis, N. (2017). Corrosion of high entropy alloys. *npj Materials degradation*, *1*(1), 15. https://doi.org/10.1038/s41529-017-0009-y

28. Senkov, O. N., Miller, J. D., Miracle, D. B., & Woodward, C. (2015). Accelerated exploration of multi-principal element alloys for structural applications. *Calphad*, *50*, 32-48. https://doi.org/10.1016/j.calphad.2015.04.009

29. Sheikh, G., & Noyan, I. C. (1989). Residual Stresses and Differential Deformation of Electroplated Structures. *Advances in X-Ray Analysis*, *33*, 161-169. https://doi.org/10.1154/S0376030800019558

30. Shi, Y., Yang, B., & Liaw, P. K. (2017). Corrosion-Resistant High-Entropy Alloys: A Review Metals. 7. https://doi.org/10.3390/met7020043

31. Soare, V., Burada, M., Constantin, I., Mitrică, D., Bădiliță, V., Caragea, A., & Târcolea, M. (2015). Electrochemical deposition and microstructural characterization of AlCrFeMnNi and AlCrCuFeMnNi high entropy alloy thin films. *Applied Surface Science*, *358*, 533-539. https://doi.org/10.1016/j.apsusc.2015.07.142

32. Walsh, F. C., & Low, C. T. J. (2016). A review of developments in the electrodeposition of tin. *Surface and Coatings Technology*, *288*, 79-94. https://doi.org/10.1109/MERCon50084.2020.9185360

33. Wang, G., Zhang, Y., Gao, C., Xu, G., & Zhao, M. (2020). Effect of residual stress and microstructure on corrosion resistance of carburised 18CrNiMo7-6 steel. *Anti-Corrosion Methods and Materials*, *67*(4), 357-366. https://doi.org/10.1108/ACMM-02-2020-2260

34. Yao, C. Z., Zhang, P., Liu, M., Li, G. R., Ye, J. Q., Liu, P., & Tong, Y. X. (2008). Electrochemical preparation and magnetic study of Bi–Fe–Co–Ni–Mn high entropy alloy. *Electrochimica Acta*, *53*(28), 8359-8365. https://doi.org/10.1016/j.electacta.2008.06.036

35. Yoosefan, F., Ashrafi, A., & Monir Vaghefi, S. M. (2022). Microstructure and corrosion properties of electrodeposited CoCrFeMnNi high entropy alloy coatings. *Frontiers in Materials*, *9*, 891011. https://doi.org/10.3389/fmats.2022.891011

36. Yoosefan, F., Ashrafi, A., Monir vaghefi, S. M., & Constantin, I. (2020). Synthesis of CoCrFeMnNi high entropy alloy thin films by pulse electrodeposition: Part 1: Effect of pulse electrodeposition parameters. *Metals and Materials International*, *26*, 1262-1269. https://doi.org/10.1007/s12540-019-00404-1

37. Yousefi, M., Rajabi, M., Reyhani, A., & Asgari, N. (2023). Corrosion and Biocompatibility Properties of TiZrNbCrV, TiZrNbFeCr, and TiZrNbFeV High Entropy Alloys Produced through Mechanical Alloying. *Journal of Materials Engineering and Performance*, 1-13. https://doi.org/10.1007/s11665-023-08990-3

38. Zhang, L.M., Yan, M.C., Zhang, S.D., Zhu, L.Y., Umoh, A.J., Ma, A.L., Zheng, Y.G., Wang, J.Q., (2020). Significantly enhanced resistance to SRB corrosion via Fe-based amorphous coating designed with high dose corrosion-resistant and antibacterial elements. *Corrosion Science*, *164*, 108305. https://doi.org/10.1016/j.corsci.2019.108305

39. Zhu, Z., Meng, H., & Ren, P. (2022). CoNiWReP high entropy alloy coatings prepared by pulse current electrodeposition from aqueous solution. *Colloids and Surfaces A: Physicochemical and Engineering Aspects*, *648*, 129404. https://doi.org/10.1016/j.colsurfa.2022.129404